International Journal of Thermophysics, Vol. 25, No. 2, March 2004 (© 2004)

Thermal Diffusivity Measurements by Photothermal and Thermographic Techniques[1]

F. Cernuschi,[2,3] P. G. Bison,[4] A. Figari,[2] S. Marinetti,[4] and E. Grinzato[4]

In this work, resulting from a collaboration between two laboratories, an analysis of different techniques to measure thermal diffusivity is presented. First, a brief description of the laser flash method, thermal wave interferometry photothermal techniques, and four different thermographic techniques in terms of experimental setups and in data processing algorithms is given. After that, results obtained on samples cut from the same block of stainless steel AISI 304 are reported. Uncertainty evaluations of the measurements are reported together with a discussion on the pros and cons of the related techniques. The agreement between the results obtained by applying the six techniques appears satisfactory from a practical point of view.

KEY WORDS: AISI 304 stainless steel; laser flash method; photothermal techniques; thermal diffusivity; thermography.

1. INTRODUCTION

A knowledge of the thermal conductivity and/or the thermal diffusivity is more and more required in many industrial fields; these are the most important properties when heat transfer processes are involved.

In the power generation industries, materials are selected primarily considering their thermal properties. The last generation of gas turbine hot path components (typically the combustion chamber, transition pieces,

[1] Paper presented at the Fifteenth Symposium on Thermophysical Properties, June 22–27, 2003, Boulder, Colorado, U.S.A.

[2] CESI, via Rubattino 54, 20134 Milano, Italy.

[3] To whom correspondence should be addressed. E-mail: cernuschi@cesi.it

[4] CNR-ITC sec. Padova, C.so Stati Uniti 4, 35127 Padova, Italy.

0195-928X/04/0300-0439/0 © 2004 Plenum Publishing Corporation

rotating blades, and vanes) are protected against the hot gases (> 1300°C) by a ceramic thermal barrier coating (TBC) with a thickness ranging from 300 μm up to 1 or more millimeters. This porous coating can drastically reduce the temperature of the internally cooled metallic base material by 100 to 300°C depending on its thickness and on its microstructure. The selection of the best insulating coating allows one to significantly increase the efficiency of the gas turbine because either the cooling flow can be reduced or a higher turbine inlet temperature (TIT) can be achieved [1].

The development of innovative ultra-high heat exchangers working at a gas temperature higher than 1400°C is strictly related to the mechanical and thermal properties of innovative ceramic matrix composites (CMC). The first prototype of heat exchangers has been realized by using high thermal conductivity ceramic materials like silicon carbide SiC/SiC or C/CSiC. Usually the value of the thermal diffusivity of the CMC has to be experimentally determined because the fibers within the components are oriented in a complex way. Therefore, a proper selection of the material with the best thermal conductivity and a suitable design of the heat exchanger piping from a thermo-mechanical point of view can be performed [2, 3].

Mechanical, electromagnetic, and thermophysical properties of metallic materials either in the form of bulk components or coatings play a key role in the development of a resonant cavity for a linear proton accelerator. In particular, the thermal diffusivity at very low temperatures of materials like copper and niobium is often required [4].

CMC SiC/SiC materials are presently under study as a possible solution for manufacturing some fusion reactor components. Also, in this case a knowledge of the thermal diffusivity of CMC can contribute to help designers in the selection of the best-suited fiber reinforced composite [5].

In the automotive and aeronautical industries, CMC materials for high performance brakes and heat shields are under development and manufacturers require, as essential information for the optimization of the brake design, the thermal diffusivity of the C/C fiber reinforced disks that have been already installed in some top car models [6].

In civil engineering, the thermal conductivity of concrete used for dams (mainly for hydroelectric power plants) or for storage tanks for liquid gases has been accurately characterized [7].

The high temperature thermal conductivity of paints is often required in lost foam casting (LFC). In fact, in LFC some refractory coatings based on mica and aluminium silicate and mica refractories are used to guarantee simultaneously high gas permeability and low thermal conductivity necessary to obtain good quality aluminium castings employing expanded polystyrene as a model for the casting [8].

Although the parameter involved in stationary heat conduction processes is the thermal conductivity λ, it is a normal practice to experimentally evaluate the thermal diffusivity α by transient methods and to calculate indirectly the thermal conductivity by the equation $\lambda = \alpha\rho C$, where the specific heat C and the mass density ρ are known.

This approach has often been proposed because the thermal diffusivity measurement is usually less time consuming and more productive, when compared with the stationary techniques used for thermal conductivity measurements; these techniques for thermal conductivity evaluation require a heat flux measurement that is long, difficult to control, and not very accurate. Moreover, the transient techniques, developed for thermal diffusivity measurement, require smaller sample dimensions and can operate over a wide temperature range. In fact, thermal diffusivity methods have been successfully applied from very low temperatures up to 3000°C.

Another advantage of measuring the thermal diffusivity instead of the thermal conductivity is related to the possibility of satisfying the condition of constant temperature during the measurement, with typical temperature variations during the measurement smaller than 1 to 2°C [9, 10].

Methods for thermal diffusivity measurements proposed over the last four decades, involve mainly photothermal and photoacoustic [11, 12] techniques. Nowadays, the laser flash method [13] is the most frequently used photothermal technique. In particular in many countries, the laser flash method is currently considered a standard for thermal diffusivity measurement of solid materials [14–16].

This method consists of heating the front face of a sample (typically a small disk-shaped specimen) by a short laser pulse and detecting the temperature evolution on its rear surface. The main advantages of this method are its simplicity and rapidity of measurement, and the possibility to measure the thermal diffusivity on a wide range of materials and within a wide temperature range. On the other hand, although the thermal diffusivity of one layer belonging to a multilayer specimen can be still determined (if the thermophysical properties and the thickness of the other layers are well known), the experimental uncertainty related to the experimental data reduction tends to increase. One other possible disadvantage of this technique depends on the requirement to extract or to manufacture a sample with well-specified dimensions and thickness. Furthermore, in some cases it is required, or at least suggested, to carry out thermal diffusivity measurements directly on components.

Other photothermal and photoacoustic techniques working in the one-side configuration (e.g., temperature monitoring is carried out on the heated surface) could, in principle, overcome these limitations. In particular, thermal wave interferometry (TWI) has been widely applied to

measure the thermal diffusivity of single and two-layer samples without any specific requirement on the sample dimensions and needing only little information about the thermophysical properties of the substrate material [17–22]. TWI in a one-dimensional approximation is based on periodic uniform heating of the front surface (typically by a modulated laser beam). The two-layer structure of coated samples (for single-layer samples, air can be fixed as a substrate) produces a change of the ac-component of the temperature with respect to an uncoated thermally thick sample that can be detected by an IR detector.

TWI in the three-dimensional approximation and the optical beam deflection (i.e., the so called "mirage") techniques have been successfully applied to measure the in-plane thermal diffusivity of bulk materials [23–30]. In both cases, the laser beam is focused on the sample surface, and by scanning the thermal wave field along positions lying outside the beam on a straight line crossing the center of the heating spot, the thermal diffusivity can be determined. The two techniques differ in the detection system. In particular in TWI, the detection of the thermal wave field is obtained by an IR detector while in the OBD, the detection is usually performed by monitoring (by a position sensor) the periodic deflection of a probe laser beam. The OBD seems to be one of the most accurate and reliable techniques, but its principal drawback is related to the sample surface preparation. As a matter of fact, a very flat and regular surface is required.

In recent years, as a result of the significant progress in infrared technology as well as in electronics, some thermographic techniques for *in situ* thermal diffusivity evaluation have been developed starting from the experience gained in the framework of photothermal techniques, whose applications are generally confined to the laboratory.

In the literature, thermographic methods used typically for measuring in-plane thermal diffusivity in bulk materials are reported. All these methods exploit in-plane heat diffusion which takes place after nonuniform heating has been imposed. Masking a portion of the sample surface during the heating [31–33] or using a spot- or line-wise heating source [34–38] are the two main ways to generate planar heat diffusion. Thermographic TWI in-plane experiments have been used to image the thermal waves and to measure the in-plane thermal diffusivity [39].

In order to verify from the end-user point of view the advantages, the limitations, as well as the uncertainty sources, the reliability, and the accuracy of some of these photothermal and thermographic techniques, a round-robin test between the Istituto per la Tecnologie della Costruzione (ITC) of the Italian National Research Council and CESI (Centro Elettrotecnico Sperimentale Italiano) has been launched. In particular, the

experimental activity has been limited to some samples extracted from the same plate of stainless steel AISI 304. The final aim of this work is to show that some of these techniques could be considered as a standard for thermal diffusivity measurements. Measurements have been carried out at room temperature for all the techniques.

2. EXPERIMENTAL TECHNIQUES

2.1. Laser Flash Method

2.1.1. Theoretical Background

The laser flash method is based on an analytical solution of the heat conduction problem within an infinite plate of thickness L, initially at a uniform temperature and uniformly heated on one surface by a Dirac (i.e., instantaneous) energy pulse. The temperature on the rear face of the plate as a function of time is

$$T(L, t) = \frac{Q}{\rho C L}\left[1 + 2\sum_{n=1}^{\infty}(-1)^n \exp\left(-\frac{n^2\pi^2\alpha t}{L^2}\right)\right] \tag{1}$$

where Q is the heating energy density. Identifying $T_\infty = \frac{Q}{\rho C L}$ as the equilibrium temperature and with $t_c = \frac{L^2}{\alpha}$, Eq. (1) can be written as

$$V(t) = \frac{T(L, t)}{T_\infty} = 1 + 2\sum_{n=1}^{\infty}(-1)^n \exp(-n^2\pi^2 t/t_c) \tag{2}$$

Figure 1 represents graphically Eq. (2).

For evaluating the thermal diffusivity, the solution proposed originally by Parker et al. [13] consisted of using the following relation:

$$\alpha = 0.1388\frac{L^2}{t_{1/2}} \tag{3}$$

where $t_{1/2}$ is the time corresponding to the half maximum increase of $V(t)$. Relationships analogous to Eq. (3) can similarly be obtained for times $t_{x\%}$ corresponding to different percentages of the maximum temperature increase [8]. An alternative approch consists of fitting the complete set of experimental data by Eq. (2). Comparison among these different methods of data reduction carried out over a wide set of experimental results has shown very good agreement when the experimental conditions fit well the theoretical assumptions [40].

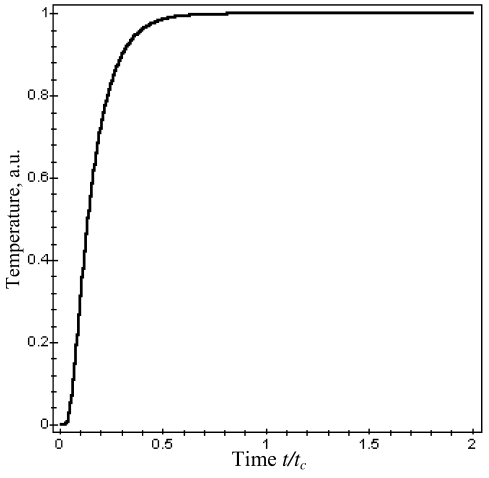

Fig. 1. $V(t)$ versus the normalized time t/t_c.

2.1.2. Experimental Setup and Results

The experimental system shown in Fig. 2 uses a pulsed 1.06×10^{-6} m wavelength Nd:YAG laser (Laser Metrics Winterpark FL-USA) as the heating source. The pulse energy can be tuned in the range 8 to 50 J. The beam shape is circular with a uniform intensity. The sample can be located within a tantalum furnace with a molybdenum shield (Theta Instruments. Port Washington, NY-USA) where it is possible to reach 1500°C. The sample and the furnace are both inside a vacuum chamber, and an infrared detector can detect the temperature of the rear face of the sample through an infrared window. The signal is then amplified, received, and processed by a PC.

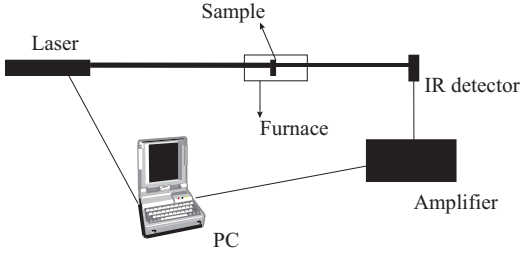

Fig. 2. Sketch of the experimental setup of the laser flash system.

Table I. Experimental and Literature Values of Thermal Diffusivity for AISI 304 Stainless Steel

Technique	Experimental value ($10^{-4}\ m^2 \cdot s^{-1}$)
Literature value (www.matls.com).	0.040
Laser flash method.	0.0399 ± 0.0006
TWI method.	0.040 ± 0.001
Method I. Spatially resolved thermography in the one-side configuration (Eq. (6)).	0.040 ± 0.005
Method I. Spatially resolved thermography in the two-side configuration (Eq. (7)).	0.040 ± 0.006
Method II. Lateral thermal wave thermography.	0.0398 ± 0.0006
Method III. One-side flash thermography.	0.040 ± 0.004

Experimental studies have been carried out on a 1×10^{-2} m diameter disk-shaped sample of 1.474×10^{-3} m thickness. Measurements have been carried out five times, and the associated uncertainty is indicated together with the average result in Table I. A typical experimental profile is shown in Fig. 3.

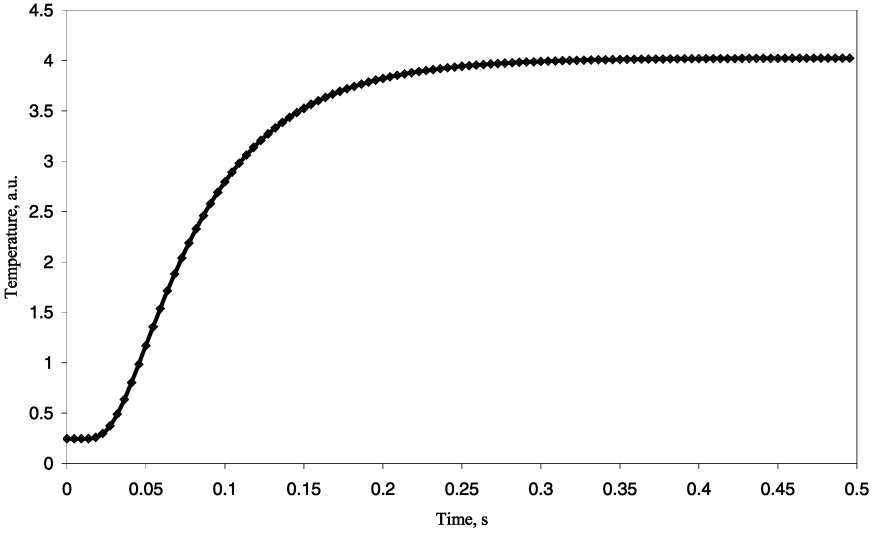

Fig. 3. Temperature increase versus time in a laser flash experiment for one of the five measurements carried out on the AISI 304 stainless steel disk-shaped sample. Dots are experimental points, and the continuous line is the fit using Eq. (2).

2.2. The TWI Method

2.2.1. Theoretical Background

Thermal wave interferometry is a well-established technique for measuring the thermal diffusivity of coatings and thin slabs. The propagation of thermal waves with angular frequency ω generated within a two-layer solid is affected by the interface between the first and second layers. In particular, thermal waves are partially reflected and transmitted at the separation surface of the two different materials like "conventional" waves. The interference between propagating and reflected waves alters the amplitude A and the phase $\Delta\phi$ of the ac component of the surface temperature,

$$T(0, t) = \frac{1}{\lambda_1 \sigma} \frac{(1 + \Gamma e^{-2\sigma L})}{(1 - \Gamma e^{-2\sigma L})} e^{j\omega t} \tag{4}$$

as follows [12]

$$A = \left(\frac{e^{4h} + 2\Gamma e^{2h} \cos(2h) + \Gamma^2}{e^{4h} - 2\Gamma e^{2h} \cos(2h) + \Gamma^2} \right)^{1/2} \qquad \Delta\phi = \arctan\left(\frac{e^{-2h}(e^{4h} - \Gamma^2)}{2\Gamma \sin(2h)} \right) \tag{5}$$

where $\sigma = (1 + j)/\mu$, and $h = L/\mu$ is the normalized thickness of the first layer. $\Gamma = \frac{\varepsilon_1 - \varepsilon_2}{\varepsilon_1 + \varepsilon_2}$ (where $\varepsilon_i = \sqrt{\rho_i C_i \lambda_i}$ is the thermal effusivity) is the thermal wave reflection coefficient at the interface where subscripts 1 and 2 refer to the first and second layers, respectively. $\mu = \sqrt{\frac{2\alpha_1}{\omega}}$ is the thermal diffusion length and represents the depth where the initial magnitude of the thermal wave is reduced by a $1/e$ factor.

Experimentally, the evaluation of the thermal diffusivity α of the first layer can be performed by fitting the experimental data acquired at different modulation frequencies with one of the two expressions of Eq. (5). The phase is usually preferred to the amplitude because it is less sensitive to optical features of the sample surface as well as to laser power variation during the measurement. As an example, Fig. 4 shows theoretical curves for the phase as a function of the normalized coating thickness h for Γ values ranging between -1 and 1 from top to bottom.

2.2.2. Experimental Setup and Results

Figure 5 shows the TWI experimental setup; the heating source was a 5 W Ar ion laser (Spectra Physics 2020). The intensity was modulated using a high stability mechanical chopper (HMS Elektronik Mod. 220-RG). The laser beam was expanded on the sample surface in order to satisfy the one-dimensional approximation. The monitoring of the ac-component of the surface temperature was performed by an $Hg_{1-x}Cd_xTe$ infrared detector

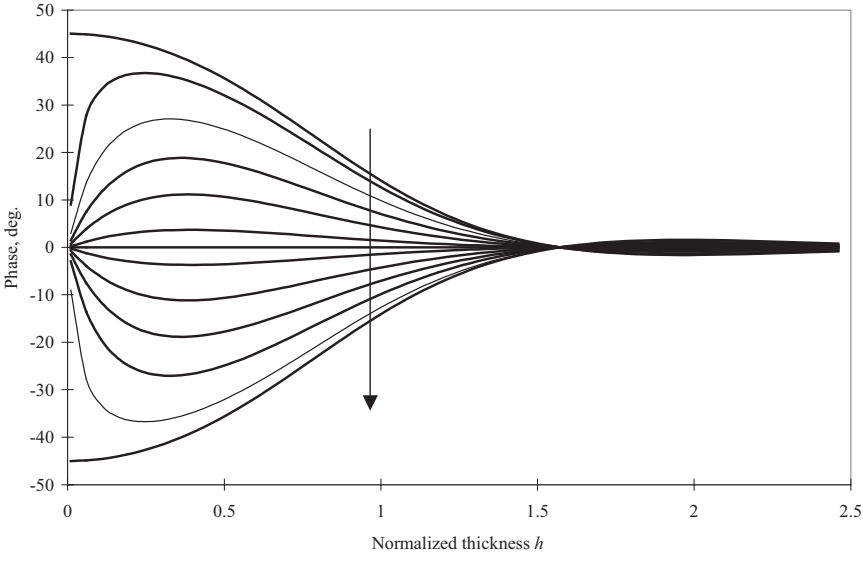

Fig. 4. Phase of the ac component of temperature versus the normalized thickness h for different values of the reflection coefficient ranging from -1 to 1 (in the sense of the arrow).

(EG&G Judson). The signal was amplified by a dc-coupled low noise transimpedance preamplifier and then by a lock-in amplifier (EG&G Mod. 5501). A time averaging procedure with a statistical treatment of the data and subsequent coating thermal diffusivity evaluation was performed under the control of a proprietary PC program.

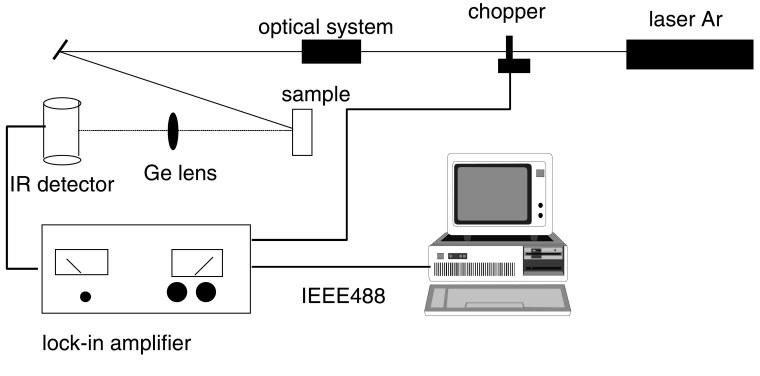

Fig. 5. TWI experimental setup.

In this specific case, measurements were carried out on a thin AISI 304 slab of 0.66×10^{-3} m thickness while modulating the heating source in a frequency range of 1 to 20 Hz as shown in Fig. 6. The uncertainty associated with the thermal diffusivity value reported in Table I is related to the standard deviation of three repeated measurements. Moreover, the statistical uncertainty of the measurement was further reduced by using protocols from Ref. 19. In particular, at each frequency thirty statistically independent phase shift values were averaged and the error bars in Fig. 6 refer to the standard deviation (always smaller than 0.5 deg) computed starting from these data. Since a single frequency scanning measurement yields a sequence of averaged data, in principle, by using the error propagation theory, it would be possible to estimate the uncertainty in the thermal diffusivity evaluation associated with a single test. However, in this work a different approach has been applied as previously explained.

2.3. Thermographic Method I (Spatially Resolved Method)

2.3.1. Theoretical Background

The temperature on the front ($z = 0$) and the rear ($z = L$) surfaces of a semi-infinite slab after an instantaneous spatially Gaussian-shaped heating pulse are, respectively, [37]

$$T(r, 0, t) = \frac{2Q}{\varepsilon \sqrt{\pi^3 t}} \sum_{n=-\infty}^{\infty} \exp\left(-\frac{((n-1)\,L)^2}{\alpha t} \frac{1}{(R^2 + 8\alpha t)}\right) \exp\left(-\frac{2r^2}{R^2 + 8\alpha t}\right) \tag{6}$$

$$T(r, L, t) = \frac{2Q}{\varepsilon \sqrt{\pi^3 t}} \sum_{n=-\infty}^{\infty} \exp\left(-\frac{((2n-1)\,L)^2}{4\alpha t} \frac{1}{(R^2 + 8\alpha t)}\right) \exp\left(-\frac{2r^2}{R^2 + 8\alpha t}\right) \tag{7}$$

Figure 7 shows the spatial distribution of the temperature as a function of the distance r from the spot center for the front slab surface at different times. Computations have been performed by using the thermal diffusivity and thermal effusivity values of AISI 304 stainless steel ($\varepsilon = 8049\ \mathrm{J \cdot m^{-2} \cdot s^{-1/2} \cdot K^{-1}}$ $\alpha = 0.04 \times 10^{-4}\ \mathrm{m^2 \cdot s^{-1}}$) and fixing the beam radius $R = 5 \times 10^{-3}$ m and slab thickness $L = 1 \times 10^{-3}$ m. The term,

$$\frac{1}{2\pi} \frac{1}{(R^2 + 8\alpha t)} e^{-\frac{2r^2}{R^2 + 8\alpha t}} \tag{8}$$

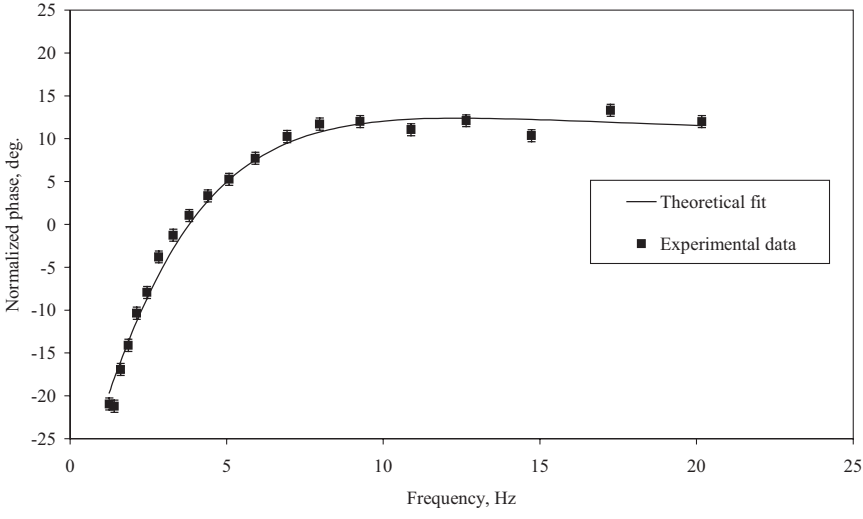

Fig. 6. Normalized phase of the ac component of the surface temperature versus the modulation frequency for the AISI 304 sample.

in Eqs. (6) and (7) is related to the finite size of the heating beam, and it is used for the measurement of the in-plane thermal diffusivity. In particular, the proposed technique consists of fitting (by using a Gaussian function), at some times, the spatial profile of the temperature along a line passing through the center of the heated spot on the front or rear sample surface

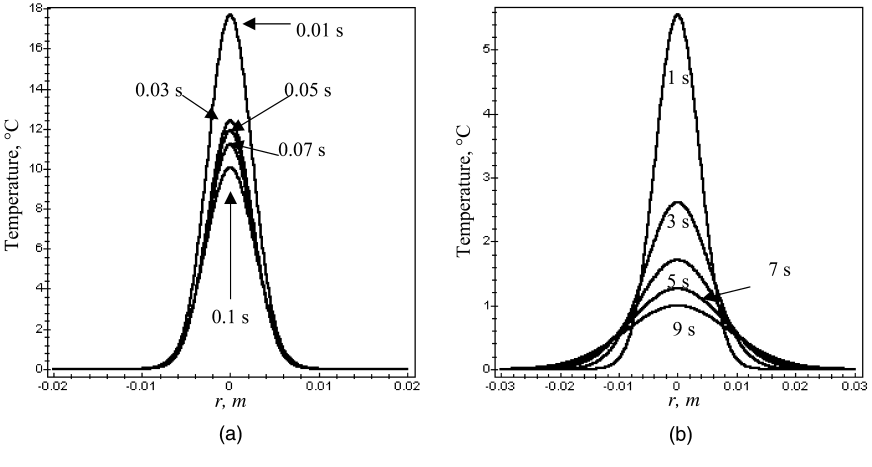

Fig. 7. Equation (6), $T(r, 0, t)$ as a function of the distance r. Curves refer to time values ranging (a) from 0.01 to 0.1 s and (b) from 1 to 9 s. Computations have been performed by using the energy $Q = 1J$ for a 1×10^{-2} m diameter Gaussian spot.

depending on the adopted configuration. In fact, the shape of the temperature profile at every fixed time depends only on the Gaussian term in Eq. (8). The angular coefficient of the straight line describing the Gaussian widening as a function of time is eight times the thermal diffusivity of the material:

$$b^2 = R^2 + 8\alpha t \tag{9}$$

Note that neither the initial time nor the beam radius and sample thickness estimation were required.

2.3.2. Experimental Setup and Results

The experimental setup consists of a 1000 W continuous lamp (PSC 1000 ILC Technology Inc., California) electronically shuttered as a heating source and of an infrared Jade focal plane array camera (CEDIP Crossy-Moligny F) sensitive in the spectral range 8 to 10×10^{-3} m for monitoring the surface temperature distribution of the sample. The sample was a 0.3×0.3 m^2 AISI 304 stainless steel plate of 1.7×10^{-3} m thickness. The measurements have been performed both in transmission (heating of front surface and temperature monitoring on the rear surface) and in reflection (heating and temperature monitoring of the front surface) configurations. The result and its uncertainty from several tests are reported in Table I. As an example, Figs. 8 and 9 show, in the one-side configuration, the temperature profile along a diameter 0.1 s after the heating pulse and linear fit of the experimental data, respectively. As far as the geometrical calibration is

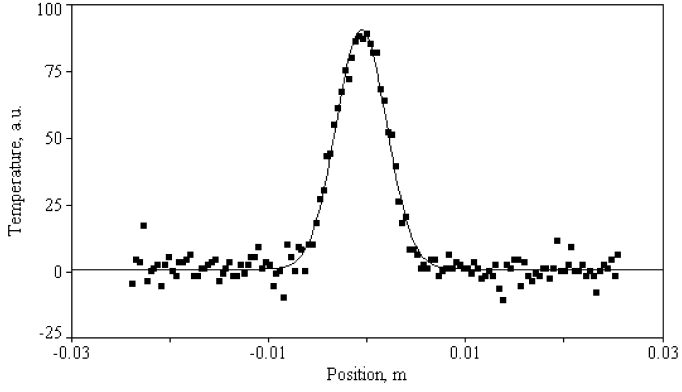

Fig. 8. Temperature versus position along a line crossing the center of the Gaussian heating spot 0.1 s after the heating. The dots are the experimental data while the best Gaussian fit (with a correlation coefficient $\xi^2 = 0.958$) is represented by the continuous line.

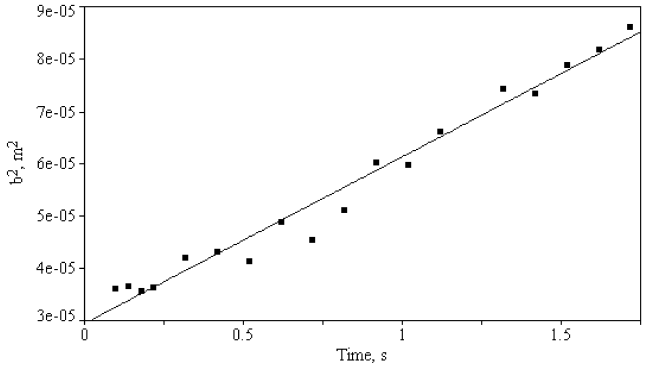

Fig. 9. The best fit of parameter b^2 as a function of time. Dots and continuous line represent the experimental data and the best fit (with a correlation coefficient $\xi^2 = 0.973$) straight line, respectively.

concerned, a razor blade has been placed on the plate surface after the experiment. This kind of blade is reflecting (thus, clearly distinguishable from the black background of the plate), and its edges are parallel and particularly sharp. The measurement has been carried out along the longest dimension in order to minimize the errors. Moreover, repeated measurements allow further reductions of the uncertainty in these measurements. In this specific case, the uncertainty related to the geometrical calibration is ± 0.5 pixels out of 110 pixels corresponding to a relative uncertainty less than 1%.

2.4. Thermographic Method II (Lateral Thermal Waves)

2.4.1. Theoretical Background

The thermal model adopted to describe the proposed experimental setup is the original one due to Ångström and presented by Carslaw and Jaeger [41–43]. It describes the temperature along a semi-infinite bar heated by a periodic source on one end, exchanging heat with the environment and being thermally thin. Therefore, the temperature varies only down to the bar (one-dimensional diffusion) according to the following equation

$$\Delta T(x, t) = \sum_{n=0}^{N} A_n \exp(-k_{1n}x) \sin(n\omega t - k_{2n}x + \psi_n)$$

$$\Delta T(x, t) = T(x, t) - T_{\text{env}} \qquad v = \frac{\gamma p}{S c_p \rho}$$

$$k_{1n} = \sqrt{\frac{v + \sqrt{v^2 + n^2\omega^2}}{2\alpha}} \qquad k_{2n} = \sqrt{\frac{v - \sqrt{v^2 + n^2\omega^2}}{2\alpha}} \tag{10}$$

where $T(x, t)$ is a temperature function depending on the x coordinate along the bar and time t, T_{env} is the environment temperature, A_n is the amplitude of the nth harmonic component, ω is the angular frequency, α is the thermal diffusivity, γ is the heat exchange coefficient, p and S are the perimeter and cross-section area of the bar, respectively, c_p and ρ are the specific heat and mass density, respectively, and ψ_n is the initial phase of the nth harmonic component.

The goal of the data reduction procedure consists of determining the spatial phase velocity k_{2n} and the attenuation coefficient of the harmonic component k_{1n}. Hence, the diffusivity α and heat exchange related parameter v are given by

$$\alpha = \frac{n\omega}{2}\frac{1}{k_{1n}k_{2n}} \qquad v = \frac{n\omega}{2}\frac{k_{1n}^2 - k_{2n}^2}{k_{1n}k_{2n}} \tag{11}$$

2.4.2. Experimental Setup and Results

A slab of AISI 304 with dimension $4\,\text{cm} \times 25\,\text{cm} \times 1.5\,\text{cm}$ is used. The height (4×10^{-2} m) is equal to the side of a thermoelectric device ($4\,\text{cm} \times 4\,\text{cm}$) that is in contact with the surface on one end of the bar. Driven by a power supply controlled by a PC, it generates the thermal waves. After some cycles, a steady regime is reached and the temperature of the surface is determined using through the IR camera (see Fig. 10 for the experimental lay-out). The acquisition is repeated at a regular time interval for some periods of the thermal wave. The temperature is finally sampled for each pixel along the propagation path of the thermal wave. As shown in Fig. 11 the sinusoidal temperature is damped and phase shifted as the space position increases. The first step of the data reduction procedure consists of time fitting the sinusoidal temperature data obtaining the amplitude and phase that depend on position. After that, a second fit with position is done on both amplitude and phase giving finally the damping factor and the phase velocity of the thermal wave. Measurements were done at different periods of the harmonic heating/cooling flux, and they are condensed in Table I.

2.5. Thermographic Method III (One-Side Flash Method)

2.5.1. Theoretical Background

It is very interesting to analyze the possibility to measure the diffusivity in the reflection mode by flash heating. The solution for the heated side of the slab is given by

$$V(t) = \frac{T(L, t)}{T_\infty} = 1 + 2\sum_{n=1}^{\infty} \exp(-n^2\pi^2 t/t_c) \tag{12}$$

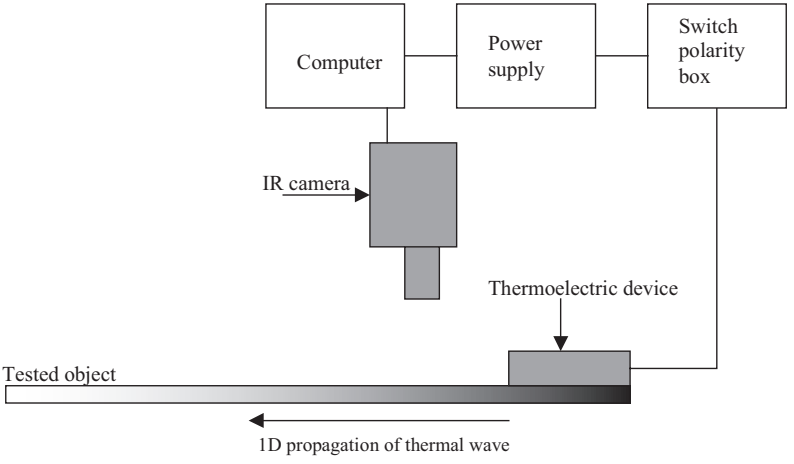

Fig. 10. Experimental setup for diffusivity measurements by thermoelectric generated thermal waves.

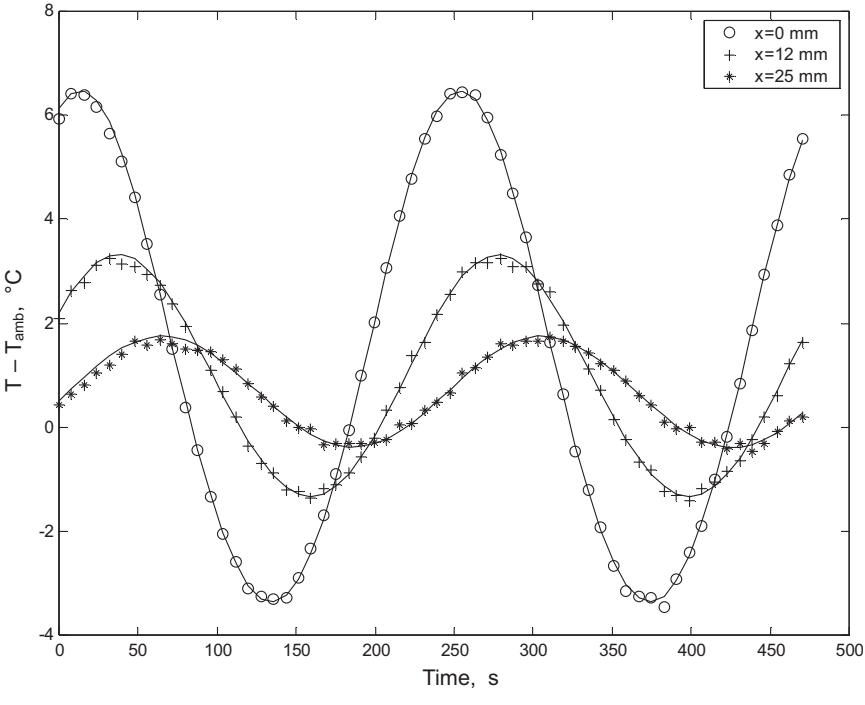

Fig. 11. Temperature versus time at increasing distances from the source/sink thermoelectric device, with fitting function superimposed (continuous line).

The lack of the term $(-1)^n$ appearing in Eq. (2) makes this solution decrease monotonically from the maximum temperature value after the flash to the T_∞ value. Unfortunately, the temperature reached during or immediately after the flash is not a reliable value to measure and, moreover, we cannot simply extract a noticeable time from the amplitude evolution much like in Eq. (2). On the other hand, it is possible to show that multiplying the solution of the front side by the cube root of the time, such a function presents a minimum (that can be measured more easily) at $\mathrm{Fo} = 0.2656$ ($\mathrm{Fo} = \alpha t / L^2$) giving the following relation for the diffusivity measurement:

$$\alpha = \frac{0.2656\, L^2}{t_{\min}} \tag{13}$$

Multiplying the temperature by the time to the nth power, provides a function that exhibits a minimum only if $0 < n < 1/2$. Indeed, using $n = 1/2$, we obtain a constant for the semi-infinite body. For the slab we obtain a nondecreasing monotonic function that is constant at the beginning of the process (like in the semi-infinite body), and goes like the square root of time when the steady condition is reached. Therefore $n = 1/3$ is the simplest choice that can be guessed to obtain a minimum to measure.

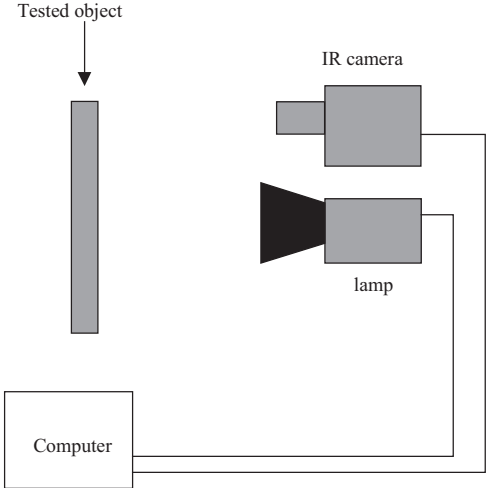

Fig. 12. Experimental setup for one-side thermal diffusivity measurement by flash heating.

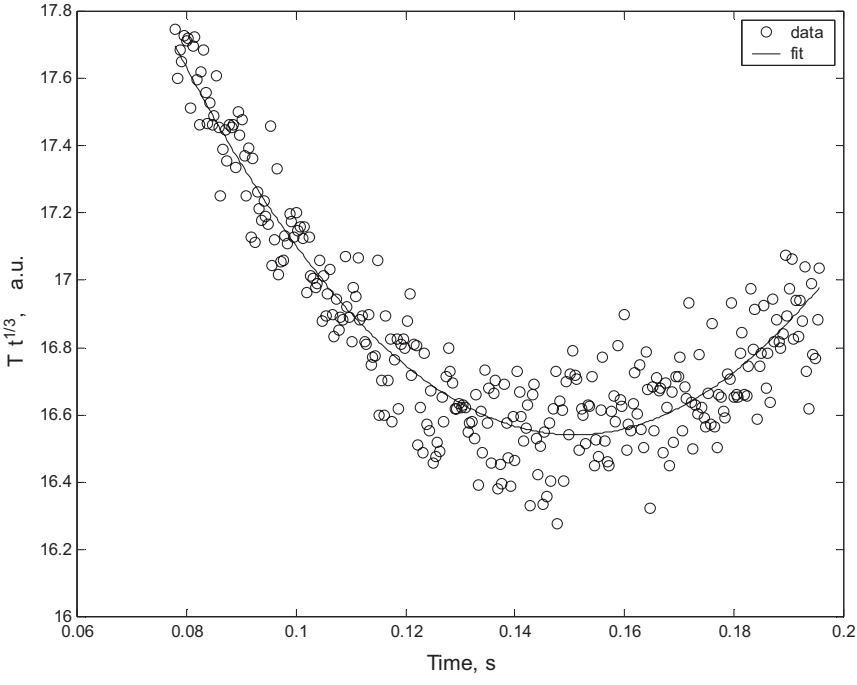

Fig. 13. Data and fitting function to obtain the time of minimum for thermal diffusivity measurement.

2.5.2. Experimental Setup and Results

The experimental setup is shown in Fig. 12. Two photographic flash lamps, 4800 J nominal energy delivered in about 10^{-2} s, heat one side of the AISI 304 slab, 1.51×10^{-3} mm thick. The temperature is determined along a line on the heated surface from an AGEMA 900 LW system for about 2 s with a sampling frequency of 2550 Hz. Figure 13 shows the plot of the function obtained multiplying the experimental temperature by the cube root of time. Results and related error obtained by error propagation of Eq. (13) are reported in Table I.

3. CONCLUSION

From the data reported in Table I, it appears that the laser flash method is the reference method for diffusivity measurements as it is currently considered. From the point of view of precision, the thermographic method II (lateral thermal waves) gives the possibility to produce thermal waves of large wavelength resulting from the Peltier

driven heat flux. That permits to exploit the capabilities of modern thermographic camera. TWI, the thermographic method III (one-side flash), and the thermographic method I (spatially resolved method) are very interesting for their practical feasibility especially for *in situ* measurements, while providing an acceptable level of precision.

From the point of view of measurement accuracy for those techniques used to measure the through-the-thickness thermal diffusivity, as already highlighted in the literature, good thickness uniformity as well as satisfactory parallelism between the sample faces are essential requirements to fit the theoretical assumptions of the analytical models. Thermographic techniques are mainly affected from the conversion factor between pixel and real length; for this reason, special care should be given to the procedures for determining this geometrical factor.

ACKNOWLEDGMENTS

The authors desire to thank Dr. D. Robba and Mr. L. Lorenzoni of CESI for their support to a part of the experimental work.

REFERENCES

1. V. P. Swaminathan and N. S. Cheruvu, "Gas Turbine Hot-Section Materials and Coatings in Electric Utility Applications", in *Advanced Materials and Coatings for Combustion Turbines*, V. P. Swaminathan and N. S. Cheruvu, eds. (ASM International, 1994).
2. European Brite-Euram Project BRPR-CT97-0425 EFCC/UHTHE/B3.
3. European Brite-Euram Project BRPR-CT97-0426 EFCC/UHTHE/B4.
4. G. Penco, D. Barni, P. Michelato, and C. Pagani, *Proc. of Particle Accelerator Conf. 2001* (Chicago, Illinois, 2001), pp. 1231–1240.
5. A. Donato, A. Ortona, C. A. Nannetti, and S. Casadio, "SiC/SiC Fibre Ceramic Composite for Fusion Application: A New Manufacturing Process," *Proc. 19th Symp. Fusion Technology (SOFT)* (Lisbon, 1996).
6. *TWI Bulletin*, Reprint 508/6/96 (Nov/Dec. 1996).
7. A. Donati, A. Lanciani, P. Morabito, P. Rossi, F. Barberis, R. Berti, A. Capelli, and P. G. Sona, *High Temp. High Press.* **19**:371 (1987).
8. T. Molibog, R. B. Dinwiddle, W. D. Porter, H. Wang, and H. E. Littleton, *American Foundrymen's Trans.* No. 00-167 (2000), pp. 471–478.
9. R. E. Taylor and K. D. Maglic, *Compendium of Thermophysical Property Measurement Methods, Vol. 1: Survey of Measurement Techniques*, K. D. Maglic, A. Cezairliyan, and V. E. Peletsky, eds. (Plenum Press, New York, 1984), pp. 299–333.
10. R. E. Taylor and K. D. Maglic, *Compendium of Thermophysical Property Measurement Methods, Vol. 2: Recommended Measurement Techniques and Practices*, K. D. Maglic, A. Cezairliyan, and V. E. Peletsky, eds. (Plenum Press, New York, 1992), pp. 281–314.
11. A. Mandelis, *Progress in Photothermal and Photoacoustic Science and Technology* (Elsevier, New York, 1991), Vol. 1, pp. 207–284.
12. D. P. Almond and P. M. Patel, *Photothermal Science and Techniques* (Chapman & Hall, London, 1996), pp. 199–220.

13. W. P. Parker, R. J. Jenkins, C. P. Butter, G. L. Gutter, and G. L. Abbott, *J. Appl. Phys.* **32**:1679 (1961).
14. ASTM C714-72, *Standard Test Method for Thermal Diffusivity of Carbon and Graphite by a Thermal Pulse Method* (ASTM, 1972).
15. BS7134: Section 4.2 (1990); *Method for the Determination of Thermal Diffusivity by the Laser Flash (or Heat Pulse) Method* (British Standards Institution 1990).
16. *JIS R 1611: Testing Methods of Thermal Diffusivity, Specific Heat Capacity and Thermal Conductivity for High Performance Ceramics by Laser Flash Method* (Japanese Standards Association, 1991).
17. P. M. Patel and D. P. Almond, *J. Mater. Sci.* **20**:955 (1985).
18. H. P. R. Frederikse, X. T. Ying, and A. Feldman, *Mater. Res. Soc. Symp. Proc.* **142**:289 (1989).
19. L. Fabbri, F. Cernuschi, P. Fenici, S. Ghia, and G. M. Piana, in *Proc. of Mater. Adv. Power Eng., Liège, Belgium*, D. Coutsouradis, J. H. Davidson, J. Ewald, P. Greenfield, T. Khan, M. Malik, D. B. Meadowcroft, V. Regis, R. B. Scarlin, F. Schubert, and D. V. Thornton, eds. (Kluwer, Dordrecht, 1994), Part II, pp. 1377–1384.
20. F. Cernuschi, A. Figari, and L. Fabbri, *J. Mater. Sci.* **35**:5891 (2000).
21. C. Wang and A. Mandelis, *J. Appl. Phys.* **85**:8366 (1999).
22. A. C. Bento, D. P. Almond, S. R. Brown, and I. G. Turner, *J. Appl. Phys.* **79**:6848 (1996).
23. G. Rousset and F. Lepoutre, *Rev. Phys. Appl.* **17**:201 (1982).
24. P. K. Kuo, M. J. Lin, C. B. Reyes, L. D. Favro, R. L. Thomas, D. S. Kim, S. Y. Zhang, L. J. Inglehart, D. Fournier, A. C. Boccara, and N. Yacoubi, *Can. J. Phys.* **64**:1165 (1986).
25. P. K. Kuo, E. D. Sendler, L. F. Favro, and R. L. Thomas, *Can. J. Phys.* **64**:1168 (1986).
26. A. Figari, *Meas. Sci. Technol.* **2**:653 (1991).
27. A. Figari, *J. Appl. Phys.* **71**:3138 (1992).
28. A. Salazar, A. Sanchez-Lavega, and J. Fernandez, *J. Appl. Phys.* **1**:1216 (1991).
29. L. Fabbri and P. Fenici, *Rev. Sci. Instrum.* **66**:3593 (1995).
30. L. Pottier and K. Plamman, *J. Phys. IV* **C7**:295 (1994).
31. J. C. Krapez, in *Proc. 5th Workshop on Advanced Infrared Technology and Applications* (Venice, Italy, 1999), pp. 289–296.
32. I. Philippi, J. C. Batsale, D. Maillet, and A. Degiovanni, *Rev. Sci. Instrum.* **66**:182 (1995).
33. Zhoung Ouyang, L. D. Favro, and R. L. Thomas, in *AIP Conf. Proc. No. 463 Photoacoustic and Photothermal Phenomena, Rome*, F. Scudieri and M. Bertolotti, eds. (AIP Woodbury, New York, 1999), pp. 374–376.
34. C. S. Welch, D. M. Health, and W. P. Winfree, *J. Appl. Phys.* **61**:895 (1987).
35. F. Cernuschi, L. Fabbri, and M. Lamperti, in *Conf. Proc. No. 463 Photoacoustic and Photothermal Phenomena, Rome*, F. Scudieri and M. Bertolotti, eds. (AIP Woodbury, New York, 1999), pp. 392–394.
36. D. He, Y. Gu, M. Zheng, and D. Zhu, *Proc. 9th Int. Topical Meeting on Photoacoustic and Photothermal Phenomena,* S. Y. Zhang, ed. (Progress in Natural Science, Nanjing, China, 1996), pp. 169–175.
37. T. Yamane, S. Katayama, and M. Todoki, *Rev. Sci. Instrum.* **67**:4261 (1996).
38. F. Cernuschi, A. Russo, L. Lorenzoni, and A. Figari, *Rev. Sci. Instrum.* **72**:3988 (2001).
39. P. G. Bison, S. Marinetti, A. Mazzoldi, E. Grinzato, and C. Bressan, *Infrared Phys. Technol.* **43**:127 (2002).
40. F. Cernuschi and L. Lorenzoni, *CESI Report No. A1/033124* (2001).
41. A. Ångström, *Philos. Mag.* **25**:130 (1863).
42. A. Ångström, *Ann. Phys. (Leipzig)* **114**:513 (1861).
43. H. S. Carslaw and J. C. Jaeger, *Conduction of Heat in Solids* (Oxford University Press, London, 1959), pp. 136–139.